

Effects of the biochar aromaticity and molecular structures of the chlorinated organic compounds on the adsorption characteristics

Lu Han¹ · Linbo Qian¹ · Jingchun Yan¹ · Mengfang Chen¹

Received: 11 October 2016 / Accepted: 19 December 2016 / Published online: 28 December 2016
© Springer-Verlag Berlin Heidelberg 2016

Abstract Adsorption behaviors of the chlorinated organic compounds (COCs) (i.e., trichloroethylene (TCE), 1,2,4-trichlorobenzene (1,2,4-TCB); 1,2-dichlorobenzene (1,2-DCB); and monochlorobenzene (MCB)) by the commercial rice husk-based biochar (RH500) and the laboratory-prepared biochars from corn stalks under different pyrolytic temperatures (i.e., CS300, CS500, CS700) were examined and interpreted by the pseudo-first-order kinetic model, the double layer model with two energies, and the Freundlich model. It is identified that the first-order adsorption rate constants ($k_1 = 0.06\sim 0.51 \text{ h}^{-1}$) were proportional to the high aromaticity and/or low polarity of biochars and the strong hydrophobicity of the COCs. The saturated adsorption capacity for the COCs was followed by the order of RH500 > CS500 > CS700 > CS300. RH500 showed the highest adsorption capacity for the COCs due to its high surface area (SA) and total pore volume (TPV). However, CS500 with low SA and TPV development highlighted the important roles of the aromaticity and/or low polarity on the COCs adsorption. In addition, 1,2,4-TCB showed the highest saturated adsorption capacity on all biochars, followed by TCE, 1,2-DCB, and MCB. The results further revealed the positive effects of the physical properties (α , N_M , ε_1 , and ε_2), the hydrophobicity and

electrostatic forces (i.e., π - π interaction and electron donor-acceptor interaction) between the adsorbates and the aromatic moieties of biochar surfaces on the adsorption of COCs.

Keywords Chlorinated organic compounds · Biochar · Adsorption · Aromaticity · Molecular structure

Introduction

Biochar is reputed to be a ubiquitous adsorbent that is produced from incompletely carbonizing of biomass in vegetation fires or pyrolysis intentionally (Ahmad et al. 2014; Cao et al. 2009; Chen et al. 2008; Lehmann 2007; Liu et al. 2015). The characteristics of large specific surface area, porous structure, profound surface functional groups, and mineral components make it efficient adsorbents for a wide range of contaminants (Bopp et al. 2016; Han et al. 2016; Koltowski et al. 2016; Qian and Chen 2013; Qian et al. 2016; Tan et al. 2015). Apart from the superior environmental functions, biochar can also help sequester carbon and improve soil fertility and reduce the mobility and bioavailability of hazardous organic chemicals (Beesley et al. 2010; Hale et al. 2011; Zhu and Pignatello 2005). Consequently, the potential environmental application of biochars may assist in diminishing the adverse effect of burning biomass wastes on the environment and helping recycle agricultural residuals (Chen and Yuan 2011; Roberts et al. 2010; Zhang et al. 2011).

Biochar is primarily composed of an amorphous phase derived from the incipient decomposition of biomass under the low heat treatment temperatures (HTTs), a composite phase with clusters of graphene sheets and changed biomolecular phase under the moderate HTTs, and highly disordered stacked graphene sheets to form a microporous network under the high HTTs (Keiluweit et al. 2010; Schmidt and Noack

Responsible editor: Guilherme L. Dotto

Electronic supplementary material The online version of this article (doi:10.1007/s11356-016-8303-8) contains supplementary material, which is available to authorized users.

✉ Mengfang Chen
mfchen@issas.ac.cn

¹ Key Laboratory of Soil Environment and Pollution Remediation, Institute of Soil Science, Chinese Academy of Sciences, Nanjing 210008, China

2000). Preponderant studies suggest that the adsorption of organic pollutants onto biochars experience a complex interaction as influenced by the char properties and molecular structure of adsorbates (Ahmad et al. 2014; Keiluweit et al. 2010; Lattao et al. 2014; Ma et al. 2011; Xiao and Pignatello 2015). The adsorption capability of a biochar largely depends on its properties, which are influenced by their pyrolytic conditions. Some of the previous studies suggest that the sequestering ability of a biochar was positively correlated to its pyrolytic temperature due to the significant enhancement in the specific surface area and the micropore volume with the increase of the HTT. However, some researchers argued that the enhancement of adsorption by chars was not necessarily related to the pyrolytic temperatures (Chun et al. 2004; Han et al. 2016; Lattao et al. 2014). For biochars prepared under the different HTTs, many factors are likely to affect the adsorption processes. Chen et al. (2008) revealed that the adsorption of organic contaminants to pine needle-based biochars was transitioned from a polarity-selective to a porosity-selective process with the increase of HTTs. Chun et al. (2004) observed that the dominant surface adsorption and a minor partition concurrently contributed to the adsorption of nitrobenzene and benzene by low-temperature chars. In addition, the adsorption might be enhanced by the effect of the micropore filling as the matching degree of molecular sizes with the pore sizes of the adsorbents was enhanced (Nguyen et al. 2007; Pelekani and Snoeyink 2000; Wang et al. 2014). Multiple molecular interactions, such as hydrophobic driving forces, electrostatic forces, and hydrogen bonding also controlled the adsorption on the surface (Ma et al. 2011; Zhu and Pignatello 2005). A number of research studies have corroborated the hypothesis that the π - π electron donor-acceptor (EDA) interaction occurred between aromatic chemicals with strong electron-withdrawing groups and polyaromatic surfaces of graphite-like biochar and carbon nanotubes with electron-rich regions (Chen et al. 2007; Fagan et al. 2004; Lattao et al. 2014; Zhu et al. 2005; Zhu and Pignatello 2005). The interaction between biochar and organic pollutants is extensively investigated; however, biochar is a complicated composite material and many factors may impact on the properties of biochar and the adsorption of organic compounds. Therefore, further studies on the effects of the aromaticity of biochars and molecular structure of adsorbates on the adsorption behavior are required.

Chlorinated organic compounds (COCs), including chlorinated aliphatic and aromatic hydrocarbons, are prevalent contaminants in China which has been detected in water, sediment, soil, and sewage sludge (Liao et al. 2014; Song et al. 2012; Song et al. 2013; Yang et al. 2014). They are widely used as degreasers, insect repellents, and intermediates in dye and pesticide synthesis (Fagan et al. 2004; Ma et al. 2011). These COCs have been listed as priority contaminants in China for its mobility in the environment and notable adverse

health effects. However, the adsorption behaviors of COCs onto biochars are still not well understood, and further studies are warranted to evaluate the effect of molecular structure of COCs on the adsorption characteristics. In addition, the reliable adsorption models play an important role in describing adsorption isotherms. The conventional models, such as the Freundlich and Langmuir model, are commonly used to analyze the adsorption data (Chen et al. 2008; Chen et al. 2012; Cotoruelo et al. 2009). However, the models are not based on physicochemical principles to interpret the adsorption process. Researches have been undertaken to use statistical physics to obtain new interpretation of the adsorption phenomena, such as the monolayer model with one energy (Hill model) and double layer model with two energies (Khalfaoui et al. 2006; Sellaoui et al. 2015, 2016). Therefore, multi-simulation methods should be considered to analyze the adsorption data. In this study, trichloroethylene (TCE), 1,2,4-trichlorobenzene (1,2,4-TCB), 1,2-dichlorobenzene (1,2-DCB), and monochlorobenzene (MCB) were chosen as representative adsorbates, due to their different molecular hydrophobicity and dimensions, to evaluate their adsorption behaviors on biochars which originated from corn stalks pyrolyzed under different temperatures in the laboratory and the rice husks commercially derived under 500 °C.

Materials and experimental methods

Materials

Biochars derived from corn stalks were collected from a local farmland in Nanjing, China. Rice husk-based biochar (RH500) was obtained from Nanjing Zhongheng Co. (Nanjing, Jiangsu Province, China). TCE; 1,2,4-TCB; 1,2-DCB; and MCB with purity greater than 99% were purchased from Sigma Aldrich. Detailed physicochemical properties of the four compounds are listed in Table S1.

Preparation of biochars

Biochars derived from corn stalks were pyrolyzed under 300, 500, and 700 °C (hereafter referred to CS300, CS500, and CS700) under anaerobic conditions, respectively. Firstly, the oven-dried corn stalks were grounded through the 0.90-mm sieve. Then, the feedstock was pyrolyzed in an electric vertical tubular furnace under an inert atmosphere (N_2) (Luo et al. 2014). In detail, the measured feedstock was tightly packed into a porcelain crucible without a lid and then placed at the bottom of the stainless steel tube. The heating speed was 5 °C/min with the flow rate of N_2 being 300 mL/min. The final pyrolytic temperature was kept for 6 h. Then, the obtained charred residues were passed through a 0.154-mm sieve with

their yields being calculated. Finally, the biochar was stored in glass bottles for subsequent experiments.

Characterization of samples

Elements including C, H, and N were analyzed by a vario MACRO CHN elemental analyzer (vario MACRO CHNS-O-CL, Elementar, Germany). The oxygen content was determined according to a mass balance (Chen et al. 2008). Surface and porous structures of biochar were determined using ASAP 2020 BET surface area analyzer (Micromeritics, Norcross, GA, USA). The functional groups of biochar were measured in the region of 4000 to 400 cm^{-1} in KBr wafers (1%) using a Fourier transform infrared (FTIR) spectrometer (Nicolet iS10, Thermo Scientific, USA). Solid-state cross-polarization magic angle-spinning ^{13}C NMR spectra were analyzed using a Bruker DSX-300 spectrometer (Karlsruhe, Germany). The detailed operating parameters were referred to Wang and Xing (2007a). The chemical shift constitutes of resonances of alkyl C (0–45 ppm); O-alkyl C (45–110 ppm) including alcohol, amines, carbohydrates, ethers, and methyl and acetal C; aromatic C-C and aromatic C-O (110–160 ppm), carboxyl C (160–190 ppm); and carbonyl C (190–220 ppm) (Liu et al. 2015; Wang and Xing 2007b).

Adsorption experiments

The experimental measurements were performed including the adsorption kinetics and isotherms of TCE; 1,2,4-TCB; 1,2-DCB; and MCB on the four selected biochars. All batch tests were performed in CaCl_2 (0.005 mol/L) to simulate environmental water using 20-mL glass vials equipped with Teflon-lined screws capped and run in triplicate. The measured

biochar samples were first added into 19 mL background solution to prewetted for 12 h. Then, an accurate volume of stock solution of a sorbate using a glass microsyringe was injected into the vials and sealed immediately. Subsequently, the vials were placed on a reciprocating shaker and agitated at 150 rpm at 25 °C. In the adsorption kinetic experiments, the initial concentration of adsorbate was approximately 5.0 mg/L for TCE and 0.4–1.0 mg/L for chlorobenzenes with biochar loading being 0.5–1.0 and 0.05–0.1 g/L, respectively. The reaction time ranged from 4 to 70 h. In the adsorption isotherm experiments, the concentration of adsorbate was 10–80 mg/L for TCE and 0.5–5.0 mg/L for chlorobenzenes with biochar loading being 0.05–1.0 g/L. During the sampling, three vials were centrifuged at 1500 rpm for 10 min to separate the char and the aqueous solution, and a 0.45- μm nylon membrane filter was used to obtain the supernatants. For TCE uptake experiments, 0.1 mL of supernatant was directly added to another clean 20-mL vial for diluting 100 times with ultrapure water. Reactor headspace samples were analyzed on a 7890 GC/5973 MSD instrument equipped with a DB-624 capillary column (30.0 m \times 0.25 mm \times 1.4 μm , Agilent). Samples were injected at 200 °C with the split ratio of 10:1. The oven temperature program was as follows: 35 °C for 2 min, 10 °C/min until 100 °C, and 25 °C/min until 220 °C for 2 min. For chlorobenzene uptake experiments, the supernatant was extracted with hexane for two times and the analysis method was referred to Han et al. (2016).

Data analysis

The pseudo-first-order kinetic model was used to fit the adsorption kinetic experimental data. The Freundlich model and the double layer model with two energies were employed to

Table 1 Yields, elemental compositions^a, atomic ratios, BET- N_2 specific surface area (SA), total pore volume (TPV), and integrated results of solid-state ^{13}C NMR spectra of the biochars

Biochar	Component/%		Elemental composition					Atomic ratio			SA m^2/g	TPV cm^3/g	
	Yield	C	H	N	O	Ash	(O + N)/C	O/C	H/C				
CS300	42.6 ± 0.1	65.28	7.84	1.43	25.45	18.32	0.24	0.39	0.12	2.87	0.013		
CS500	31.8 ± 0.3	79.57	5.16	1.40	13.87	25.11	0.41	0.17	0.070	7.11	0.016		
CS700	28.6 ± 0.5	83.11	3.78	1.46	11.66	27.85	0.19	0.14	0.045	13.16	0.026		
RH500	–	77.19	4.52	0.58	17.71	36.72	0.24	0.23	0.059	205.35	0.11		
Biochar	Distribution of C chemical shift, ppm (%)										Total polar aromatic C (%)	Total polar C (%)	Aliphatic polar C (%)
	Alkyl C	O-alkyl C	Aromatic C-C	Aromatic C-O	Carboxyl C	Carbonyl C	Aliphatic C (%)	Total aromatic C (%)	Total polar C (%)	Aliphatic polar C (%)			
	0–45	45–60	60–90	90–110	110–140	140–160	160–190	190–220	0–110	110–160	45–110 and 140–220	45–110	
CS300	29.73	6.73	12.70	4.43	24.87	12.49	5.86	3.18	53.59	37.37	45.40	23.86	
CS500	3.38	0.39	0.00	0.38	77.71	16.05	2.02	0.07	4.16	93.75	18.91	0.78	
CS700	1.33	1.82	6.15	12.38	67.92	8.70	1.70	0.00	21.68	76.62	30.75	20.35	

^a Elemental compositions and atomic ratios are on the basis of ash deducted. H/C, O/C, and (O + N)/C are atomic ratios of various elements to carbon

analyze the adsorption isotherm data. The theoretical basis of double layer model with two energies was referred to Sellaoui et al. (2016). These models were detailed in the “Supporting Information.”

Results and discussion

Characteristics of biochars

The yields, elemental compositions, atomic ratios, BET-N₂ specific surface area (SA), and the total pore volume (TPV) for biochar samples are displayed in Table 1. The yield of corn stalk-based biochar was declined with the increase of HTTs from 42.6 to 28.6%, similar to those reported for corn stalk-based biochars (Fu et al. 2009; Luo et al. 2014) and higher than those reported by Xiao et al. (2013). The observed reduction in the yield from CS300 to CS500 was attributed to the loss of the volatile matter during the pyrolysis of cellulose and hemicellulose (Cao et al. 2012). With HTTs from 300 to 700 °C, the content of C was increased substantially by 27.31% due to the accumulation of the fixed C being formed in the carbonization process (Keiluweit et al. 2010), while H and O contents were decreased from 7.84 to 3.78% and from 25.45 to 11.66%, respectively. The content of N is relatively stable during the carbonization and generally higher than that of wood chars without respect of temperature (Wang et al. 2013). RH500 was different in the elemental compositions from CS500 and displayed strong aromaticity and hydrophobicity owing to its lower H/C and (O+N/C) atomic ratios. The ash contents of the biochars derived from corn stalks and rice husks were in the range from 18.32 to 36.72%. As presented in Table 1, the SA of different biochars ranged from 2.87 to 205.35 m²/g, which is in accordance with the nitrogen adsorption-desorption isotherms of biochars shown in Fig. S1a. However, the development in SA and TPV of corn stalk-derived biochars with the increase of HTT was not as markedly as other reported literatures (Keiluweit et al. 2010; Liu et al. 2015; Zhang et al. 2011). One possible explanation may be that corn stalks were not intrinsically microporous or that the prevalent pores within these chars were small and dead ended, making the adsorption gas inaccessible (Fu et al. 2009). In addition, the corn stalk biochar was synthesized in a vertical stainless steel tube (φ10 × 110 cm) with a narrow core vent (φ3 cm) in the study. The high HTT (>500 °C) and poor exhaust conditions in the tube are likely to result in high pressure, making the porous structure cracked and partially closed due to the softening and melting of the feedstock over the pyrolytic process. This phenomenon on low surface area and porous structure of biochar was also documented by other studies (Sharma et al. 2002; Lee et al. 2010; Liu et al. 2010). The pore size distribution for corn stalk-derived biochars as obtained with the BJH method

(Fig. S1b) ranged from 3 to 5 nm, mainly belonging to mesopores (2–50 nm), while RH500 contained a great number of micropores (<2 nm) and mesopores.

The FTIR spectra of CS300, CS500, CS700, and RH500 are presented in Fig. 1a. The presence of functional groups on biochar samples is referred to the documented literatures (Chen et al. 2008; Fu et al. 2009; Keiluweit et al. 2010; Pastor-Villegas et al. 2007). CS300 exhibited abundant surface functional groups, such as –OH stretching vibration within the vicinity of 3400 cm⁻¹ belonging to the dehydration of cellulosic and ligneous components; –CH₂ stretching vibration at 2922, 2854, and 1451 cm⁻¹ assigning to nonpolar aliphatic fractions in biopolymers; –CH₃ stretching vibration near 1375 cm⁻¹ (1399 and 1384 cm⁻¹); ester C=O stretching vibration at 1734 cm⁻¹ mainly associated with carboxyl, trace of aldehydes, ketones, and esters; aromatic skeletal C=C and C–O stretching vibrations at 1613 and 1514 cm⁻¹; aliphatic C–O–C and alcohol–OH stretching vibrations between 1163 and

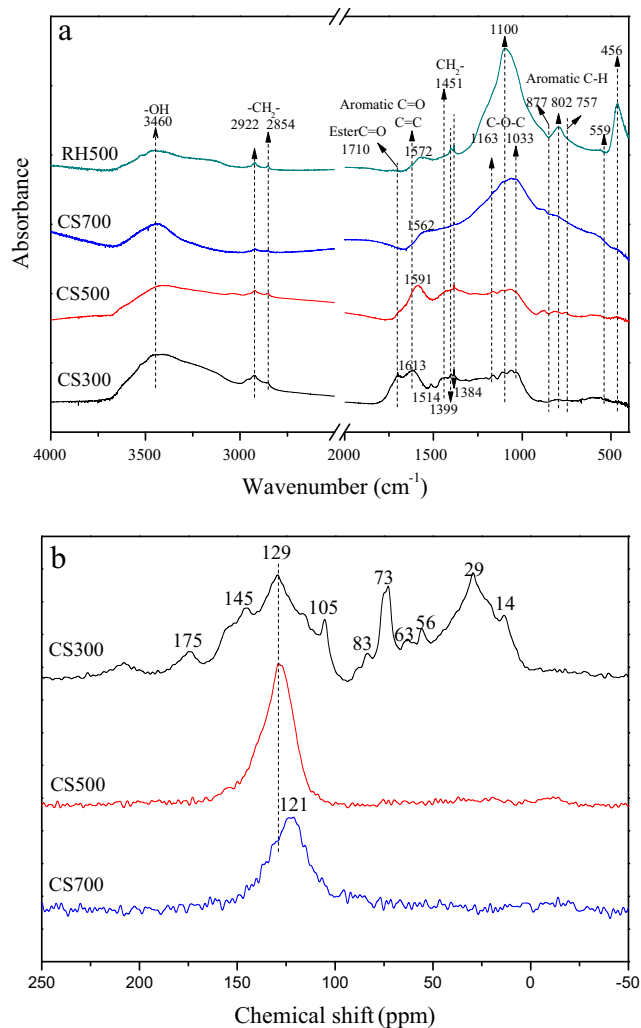


Fig. 1 Fourier transform infrared (FTIR) spectra (a) and solid-state ¹³C NMR spectra (b) of the biochars

1033 cm^{-1} belonging to ether-type structures in the corn stalk; and C-O stretching vibrations at 1033 and 1100 cm^{-1} attributable to primary C-OH and secondary O-H. With the further increase of HTT, the stretching vibrations of $-\text{CH}_2$ (2922 and 2854 cm^{-1}) and polar groups (C-O, ester C=O and $-\text{OH}$) were eliminated remarkably on CS500 and almost completely disappeared on CS700. These are well correlated with the decrease of the H and O contents. However, signals of 1451, 1399, and 1384 cm^{-1} did not diminish markedly, combined signals of aromatic skeletal C=C and C=O bands (1591 cm^{-1}), which indicated that CS500 could contain a number of aromatic compounds (Li et al. 2014). In addition, the presence of aromatic C-H stretching vibrations at 877, 802, and 757 cm^{-1} denoted the increase of aromatic fractions and the enhancement of carbonization degree (Keiluweit et al. 2010). The elimination of absorption peaks near 1600 cm^{-1} for CS700 is likely due to the destruction of lignin residues. The remarkable peaks at 1163–1033 cm^{-1} for CS700 are associated with C-O and C-C stretching, which are ascribed to the exposure of the aromatic cores from the lignin residues at the high HTT (Chen et al. 2008). Han et al. (2016) also identified the intensified absorption peak at 1150 cm^{-1} for the carbonization of lignin, which may be due to the crystallization of lignin under the high HTT. Evolutions in aliphatic and aromatic carbon contents will be further discussed in next paragraph with the NMR spectra. RH500 showed similar absorption peak signals to CS500, except that the moderate signal at 1572 cm^{-1} representative of less aromatic moieties and the remarkable

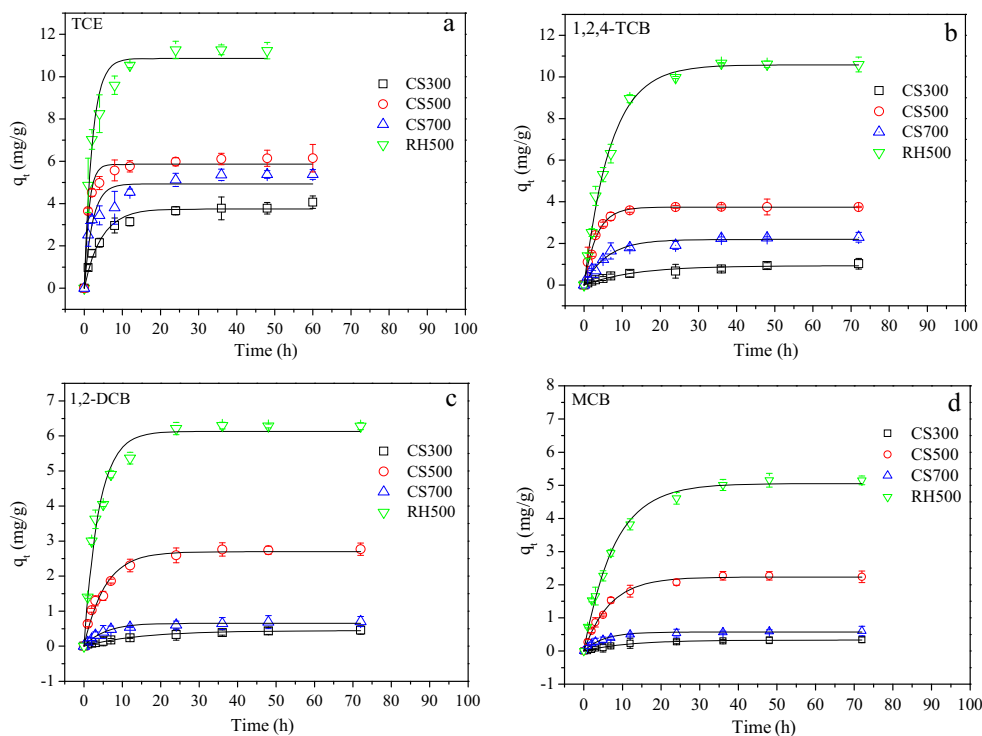
signals at 1100, 802, and 465 cm^{-1} were caused by more silicon components (Qian and Chen 2013).

The ^{13}C NMR spectra and integrated results of CS300, CS500, and CS700 are shown in Fig. 1b and Table 1, respectively. CS300 showed the presence of substantial alkyl and O-alkyl groups from the multiple peaks located at 0–45 and 45–110 ppm and a few total aromatic C (110–160 ppm), which are typically attributable to cellulose, hemicellulose, and lignin components (Baldock and Smernik 2002). With the increase of HTT, aromatic C structures constitute the main component of biochars produced (Chen et al. 2014). A notable development in the well-defined aromatic C resonance centered at 129 ppm is observed in the NMR spectra of CS500. Additionally, CS700 shifted to relatively low chemical shift to 121 ppm. This is simultaneous with the attenuation of signals corresponding to the aliphatic C and total polar C and aliphatic polar C contents, as shown in Table 1, demonstrating the increased hydrophobicity. It should be noted that CS500 contained the highest content of total aromatic C and the lowest total polar C, which is consistent with the outcome of FTIR spectra; however, further investigation is required to explain this phenomenon.

Adsorption kinetic experiments

The adsorbed amounts of the representative four COCs onto the selected biochars as a function of time are presented in Fig. 2. The apparent equilibrium time was 48 h. The pseudo-

Fig. 2 Adsorption kinetics of chlorinated organic compounds onto biochars. The *solid curves* are fitted by the pseudo-first-order kinetic model



first-order model was used to fit the adsorption kinetic data (Table S2) with the correlation coefficients (R^2) between 0.878 and 0.995. The pseudo-first-order adsorption rate constants (k_1) ranged from 0.06 to 1.14 h⁻¹, and TCE commonly had higher k_1 values than chlorobenzenes on biochars. The adsorption of organic compounds onto natural sorbents and synthetic polymers has been considered a complex process, which is ultimately related to the biochar textures and the properties of adsorbates (Ahmad et al. 2013). As shown in Fig. S2a, k_1 values are plotted as a function of different biochars. It is observed that different COCs showed a variety of k_1 values on distinct biochars, and all the COCs had a maximum k_1 value on CS500. The SA and TPV in RH500 were approximately one order of magnitude larger than those in CS500 (Table 1), but with lower rate constants of the COCs. As RH500 had lower carbonization degree than CS500 from the FTIR data, it is inferred that the rate constants of the COCs are likely related to the surface chemical composition. Thereafter, k_1 values are also compared with the contents of total aromatic C and the total polar C from the NMR data of corn stalk-based biochar (Fig. S2b–c). The results indicated

that the strong aromaticity and hydrophobicity of CS500 facilitated the accessibility of the COCs to biochars. The positive correlation between the adsorption of hydrophobic compounds with the carbonization was also reported by others (Chen et al. 2012; Chio and Al-Abed 2009; Cabal et al. 2009). In addition, there are discrepancies on the rate constants from different COCs on the same biochar; in particular, k_1 of TCE was markedly higher than those of chlorobenzenes. This suggested that the adsorption of the aqueous phase to carbonaceous sorbents could be impacted by hydrophobicity and/or molecular structure of adsorbates. Fig. S2d illustrates the k_1 constants plotted as functions of the octanol-water partition coefficient ($\log K_{ow}$). It is observed that k_1 values of the COCs are positively correlated with the $\log K_{ow}$, except for TCE ($\log K_{ow} = 2.42$), which could explain why chlorobenzenes having strong hydrophobicity are readily attractive to the surfaces of biochars. For TCE molecular structures, its strong mobility associated with the highest aqueous solubility and the smallest molar volume (1280 mg/L and 89 mL/mol in Table S1) is likely to lead to the high rate constants (Ahmad et al. 2013). Thus, the adsorption kinetics of COCs are largely

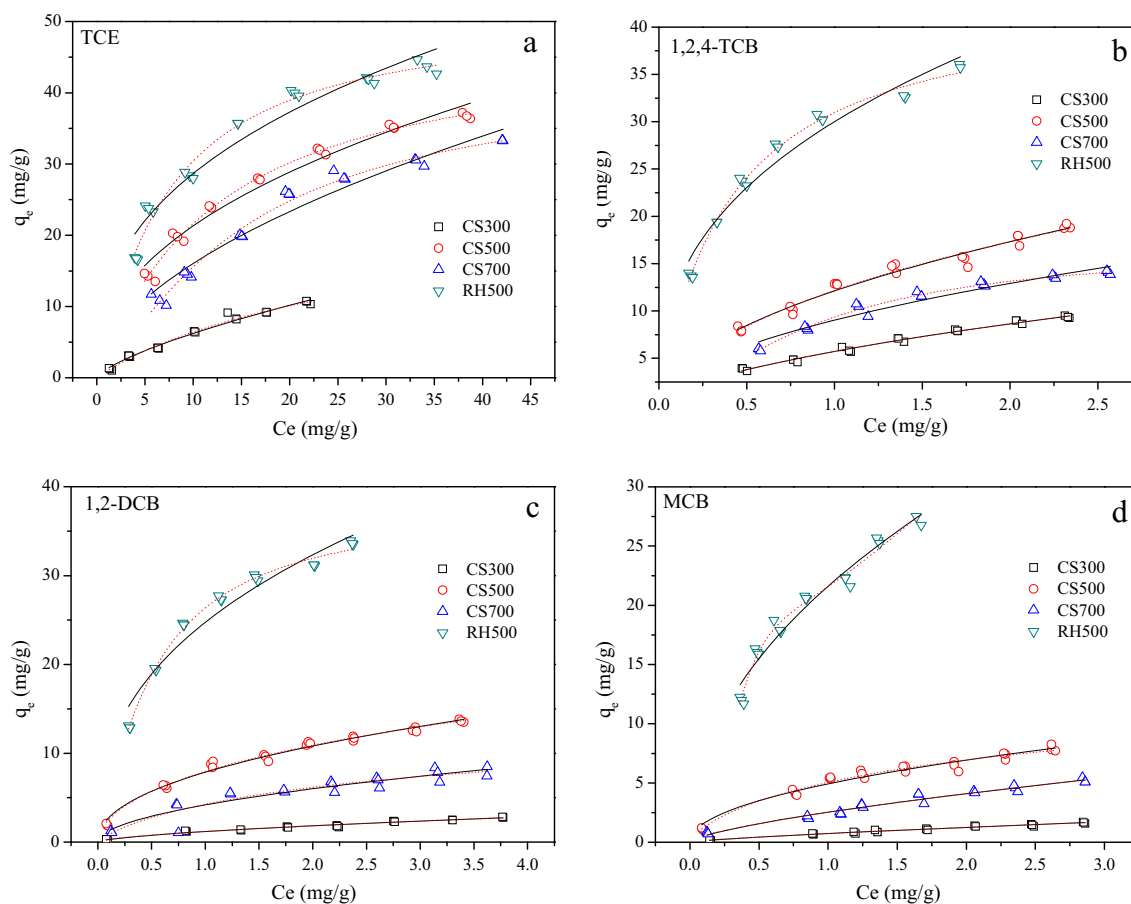


Fig. 3 Adsorption isotherms of chlorinated organic compounds on the biochars. The *solid curves* and the *dotted curves* are fitted by the Freundlich model and the double layer model with two energies,

respectively. The concentration of adsorbate was 10–80 mg/L for TCE and 0.5–5.0 mg/L for chlorobenzenes with biochars loading being 0.05–1.0 g/L. The experimental temperature was 25 °C

dependent on the aromatic composition of biochar and molecule structures of COCs.

Adsorption isotherm experiments

The outcome of the adsorption isotherms The adsorbed amounts of the four COCs on biochars were decreased in the order of RH500 > CS500 > CS700 > CS300 under the adsorption equilibrium (Fig. 3). A notable discrepancy on the adsorption ability was observed between the corn stalk- and the rice husk-based biochars. The different feedstocks of biomasses are thought to be responsible for biochars exhibiting a variety of adsorption capacities. It could be attributable to the great development in SA and the pore volume for RH500, which provided high-energy adsorption sites and pore-filling space for the adsorption of organic compounds (Nguyen et al. 2007; Ran et al. 2013; Wang et al. 2014). Corn stalk-based biochars contained relatively low SA and TPV, and a moderate enhancement in SA and TPV was observed with the increase of the HTT. However, the adsorption capacity of biochars did not exhibit a positive correlation with SA or TPV. It is identified that the highest adsorbed amounts on CS500 were observed for all the four COCs.

The model fitting results The adsorption isotherms of the COCs on different biochars fitted by the double layer model with two energies and the Freundlich model are shown in Fig. 3. The parameters, including the number of molecules per site (α), the density of receptor sites (N_M), the adsorbed

quantity at saturation (q_0) and the calculated values of adsorption energies (ε_1 and ε_2), fitted using the double layer model with two energies are presented in Table 2. The modelling results allowed new physical interpretation at microscopic levels. The coefficient R^2 ranged from 0.851 to 0.992. α values for the COCs' adsorption on different biochars ranged from 0.56 to 1.22. According to the multi-molecular adsorption mechanism and the multi-anchorage adsorption mechanism, α value could be greater or smaller than one, which represents the number of adsorbed molecules per site or the fraction of molecule per site, respectively (Khalfaoui et al. 2003; Knani et al. 2007). Therefore, $1/\alpha$ indicating the number of receptor sites to adsorb one molecule (if $\alpha < 1$) (Ben Yahia et al. 2013) as a function of different COCs adsorption on biochars is shown in Fig. S3a. The number of receptor sites to adsorb one molecule was increased in the order of TCE < 1,2,4-TCB < 1,2-DCB < MCB, implying that less adsorption sites were needed to capture TCE and 1,2,4-TCB molecules. Fig. S3b depicts the evolution of adsorbed quantity at saturation (q_0 calculated by $2\alpha \times N_M$) as a function of different COCs adsorption on biochars. The q_0 value of the four COCs on biochars followed the order of RH500 > CS500 > CS700 > CS300, which is consistent with the results illustrated in Fig. 3. In addition, 1,2,4-TCB showed the highest q_0 on all the biochars, followed by TCE, 1,2-DCB and MCB. This finding was mainly attributable to all the biochars showing the highest N_M value for adsorbing 1,2,4-TCB (Table 2). Furthermore, the sum of the ε_1 and ε_2 for 1,2,4-TCB showing relative lower values indicated that less adsorption energy was

Table 2 Parameters of the adjustment with the double layer model with two energies

Biochar	Adsorbates	Double layer model with two energies					
		α	N_M (mg/g)	q_0 (mg/g) ^a	ε_1 (kJ/mol)	ε_2 (kJ/mol)	R^2
CS300	TCE	0.77	13.99	21.45	10.29	10.03	0.985
	1,2,4-TCB	0.66	68.42	89.70	9.67	8.62	0.985
	1,2-DCB	0.59	21.69	25.77	8.09	6.64	0.978
	MCB	0.56	13.16	14.66	9.31	7.42	0.971
CS500	TCE	0.75	32.06	48.40	12.47	11.51	0.988
	1,2,4-TCB	0.62	92.76	114.11	10.77	8.56	0.966
	1,2-DCB	0.67	25.32	34.10	10.62	6.72	0.990
	MCB	0.57	23.87	27.35	9.84	8.89	0.969
CS700	TCE	0.95	22.22	42.43	10.84	10.96	0.979
	1,2,4-TCB	0.75	71.23	106.96	9.48	9.14	0.983
	1,2-DCB	0.72	21.08	30.36	9.99	7.73	0.851
	MCB	0.70	39.93	55.91	10.52	7.93	0.963
RH500	TCE	0.96	45.48	87.45	15.31	13.35	0.977
	1,2,4-TCB	0.75	79.58	119.50	11.27	10.93	0.990
	1,2-DCB	1.11	37.37	82.80	14.83	13.30	0.992
	MCB	1.22	6.18	15.04	14.48	13.74	0.976

^a $q_0 = 2\alpha \times N_M$ was referred to Sellaoui et al. (2016)

Table 3 Parameters for the Freundlich isotherm model

Biochar	Adsorbates	Freundlich model		
		K_f (L ⁿ /mg ⁿ⁻¹ g)	n	R^2
CS300	TCE	1.21	0.71	0.983
	1,2,4-TCB	5.74	0.59	0.986
	1,2-DCB	1.20	0.62	0.979
	MCB	0.73	0.77	0.973
CS500	TCE	7.81	0.43	0.966
	1,2,4-TCB	12.13	0.52	0.969
	1,2-DCB	7.88	0.46	0.984
	MCB	4.93	0.49	0.965
CS700	TCE	4.64	0.54	0.950
	1,2,4-TCB	9.04	0.52	0.948
	1,2-DCB	4.19	0.52	0.861
	MCB	2.53	0.69	0.966
RH500	TCE	12.00	0.43	0.940
	1,2,4-TCB	30.00	0.38	0.959
	1,2-DCB	24.74	0.39	0.947
	MCB	21.62	0.47	0.955

needed for biochar to anchor it, which was also likely to be responsible for its highest saturated adsorption capacity (Fig. S3c).

The parameters for the Freundlich model are summarized in Table 3 with the coefficient (R^2) between 0.861 and 0.986. The adsorption affinity coefficients (K_f) of the COCs were in the range of 0.73 to 30.00 Lⁿ/mgⁿ⁻¹ g, and RH500 commonly had the highest K_f values for the COCs. The adsorption isotherms for the COCs are nonlinear on all the biochars, with nonlinearity index (n) ranging from 0.77 to 0.38, indicating a heterogeneous and nonuniform adsorption. It is also worth noting that CS500 showed the highest level of K_f and n from biochars derived from corn stalks (Fig. S4a–b). This finding indicated that the SA and pore volume of biochar are not major determinant for the sorption of organic compounds to carbonaceous materials, particularly for biochars with a poor development in SA and TPV. Previous study has discovered that the polar organic compound such as nitrobenzene is inclined to approach to the polar fractions of biochar under the low HTT (Chun et al. 2004). Lattao et al. (2014) also identified that the adsorption intensities of benzene, naphthalene, and 1,4-dinitrobenzene were maximized on the 500 °C wood

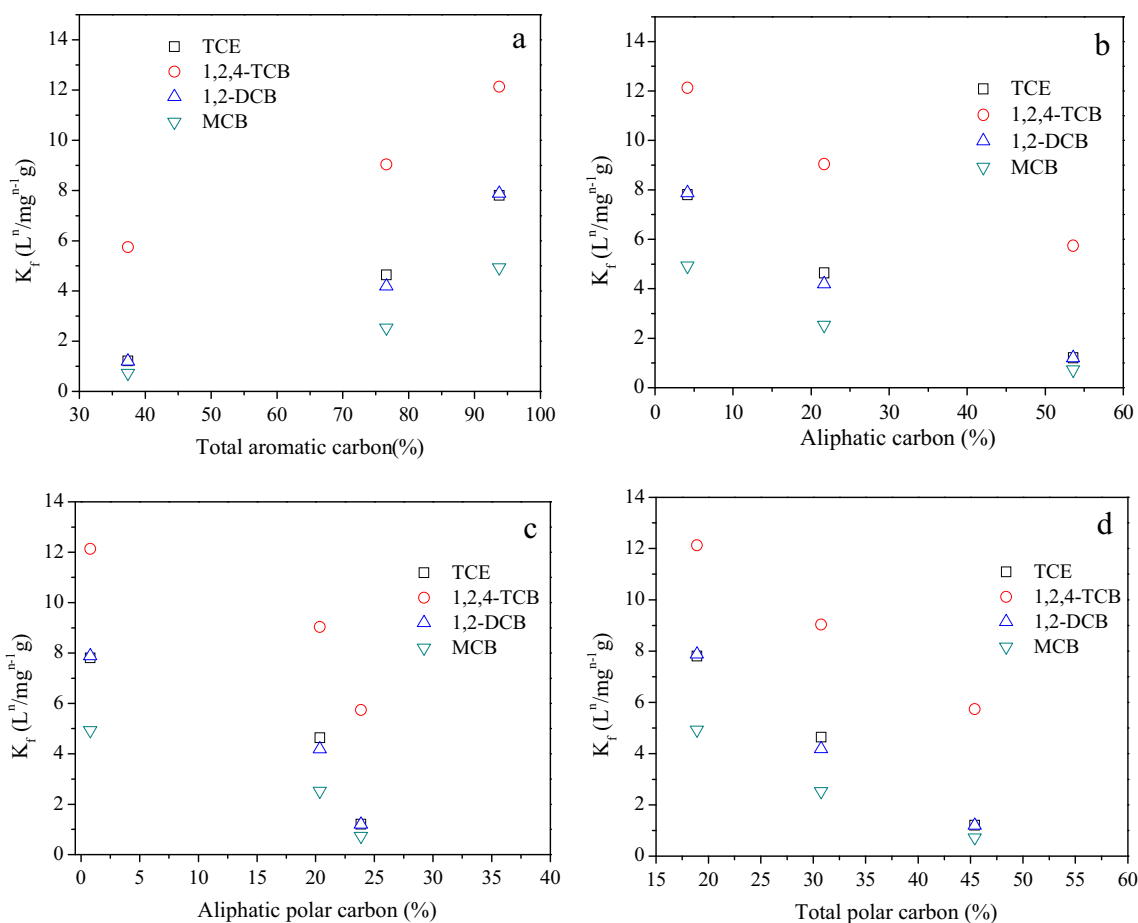


Fig. 4 Relationship between the Freundlich adsorption affinity coefficients (K_f) and the total aromatic C content (a), the aliphatic C content (b), the aliphatic polar C content (c), and the total polar C content (d)

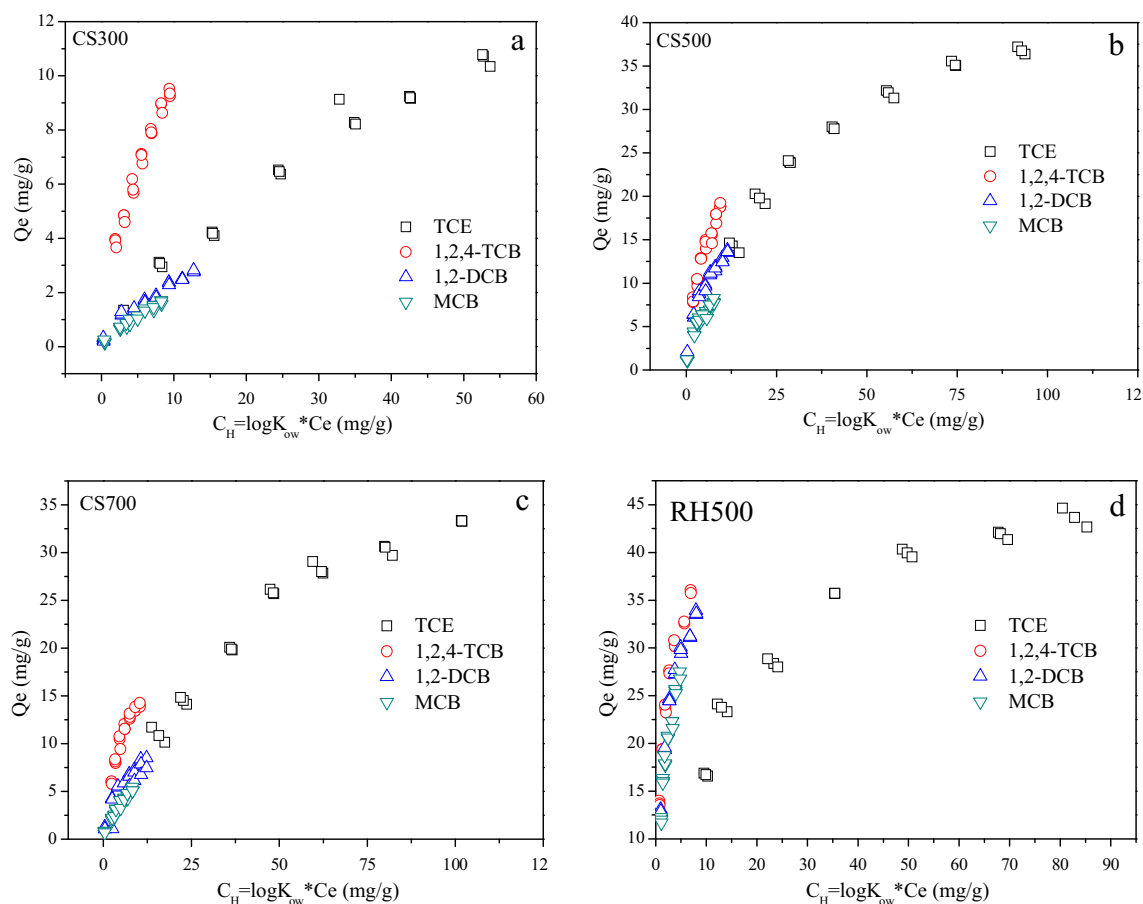


Fig. 5 Octanol-water partition coefficient ($\log K_{ow}$) normalized adsorption isotherms of chlorinated organic compounds on biochar

char from those chars derived from the HTTs between 300 and 700 °C. Han et al. (2016) identified that the hemicellulose-based biochar, showing the lowest surface area and pore volume among those derived from cellulose, hemicellulose, and lignin, had the second greatest sorption capacity. Therefore, additional factors should have been operated to influence the sorption ability of CS500.

The effect of chemical composition of biochars on the adsorption The relationship between the K_f of the different COCs and the content of total aromatic C (the content of aliphatic C) in biochars is illustrated in Fig. 4a, b. It is noticeable that K_f was positively correlated with the percentage of total aromatic C and inversely correlated with the percentage of aliphatic C, with the highest sorption affinity of COCs being displayed on CS500. The debates on the roles of aliphatic and aromatic groups within the adsorbents on the adsorption of organic compounds are still ongoing (Chefetz et al. 2000; Chefetz and Xing 2009). Comparable studies highlighted the importance of both aromatic-rich (Xing 2001; Keiluwit et al. 2010; Wang and Xing 2007a, b) and aliphatic-rich (Chefetz 2003; Chun et al. 2004; Kang and Xing 2005; Sun et al. 2012) adsorbents for the sorption of hydrophobic organic compounds. In the present study, the representative

adsorbates belong to planar apolar hydrophobic organic compounds with C=C double bond and benzene ring structure (Zhu et al. 2004; Zhu et al. 2005). They are likely to be accessible to the hydrophobic aromatic cores on biochars by π - π interactions (Ma et al. 2011; Wang et al. 2014; Xiao and Pignatello 2015; Zhu et al. 2004). Therefore, this finding suggested that aromatic-rich biochars favored the adsorption of the COCs. The negative relationship between K_f and the content of aliphatic polar C (Fig. 4c) or the total polar C (Fig. 4d) further suggested that the high polarity of biochar could adversely affect the adsorption of the COCs. It is inferred that the COCs are likely to be masked by the surrounding oxygen-containing groups of biochars and thus inaccessible to the surface of biochar (Chen and Xing 2005; Wang et al. 2007). As a result, adsorbents with the high extent of aromaticity and low polarity have a high affinity for the hydrophobic COCs.

The effect of the COCs' property on the adsorption The COCs' adsorption on biochars is also likely governed by multiple intermolecular forces, such as hydrophobic forces and electrostatic forces (Ma et al. 2011). It is clear that the hydrophobicity of the COCs contributed to the adsorption ability, since the adsorbed amounts of chlorobenzenes were positively correlated with their hydrophobicity. However, TCE with

relative low hydrophobicity showed higher adsorption capability than chlorobenzenes, indicating that the hydrophobicity of COCs is not necessarily dominant on the adsorption process. The adsorption isotherms of COCs on biochars normalized with $\log K_{ow}$ are presented in Fig. 5, in which $C_H = C_e \times \log K_{ow}$, where C_H is *n*-hexadecane as a reference solvent. It is observed that the adsorbed amounts of COCs normalized by $\log K_{ow}$ were decreased in the order of 1,2,4-TCB > TCE > 1,2-DCB \approx MCB, except RH500, indicating that high-chlorinated compounds are more readily accessible to biochar than low-chlorinated compounds. The electrostatic forces, such as π - π interaction, as mentioned previously, may contribute to the adsorption. Furthermore, as the -Cl is a typical electron acceptor, and the aromatic moieties on biochar surface can serve as an electron donor (Ma et al. 2011). Thus, an electron donor-acceptor (EDA) interaction may explain the stronger affinity of highly chlorinated compounds adsorption to biochars than lowly chlorinated compounds. For 1,2,4-TCB and TCE, the molecular size of 1,2,4-TCB (4.9 Å) is smaller than TCE (5.6 Å) (Li et al. 2002; Nguyen et al. 2007), indicating a smaller steric hindrance by micropore-filling sorption. Therefore, the adsorption of COCs onto biochars is also greatly affected by their molecular structures.

Conclusions

In this work, the four COCs adsorption on different biochars was investigated and interpreted by the pseudo-first-order kinetic model, the double layer model with two energies, and the Freundlich model from the physical and chemical point of view at microscopic level. It is identified that the high aromaticity and/or low polarity of biochars and the strong hydrophobicity of the COCs could enhance the adsorption rate constants of the COCs. The q_0 for the COCs was followed by the order of RH500 > CS500 > CS700 > CS300. RH500 showed the highest adsorption capacity for the COCs as related to its high SA and TPV; whereas, the corn stalk-based biochars, with low SA and TPV development, highlighted the important roles of the aromaticity and/or low polarity on the uptakes of the COCs. In addition, 1,2,4-TCB showed the highest q_0 on all biochars, followed by TCE, 1,2-DCB and MCB. The results further revealed the positive effects of the physical property (α , N_M , ε_1 , and ε_2) and the hydrophobicity and electrostatic forces (i.e., π - π interaction and electron donor-acceptor interaction) between the adsorbates and the aromatic moieties of biochar surfaces on the adsorption of COCs.

Acknowledgements The National High Technology Research and Development Program of the Ministry of Sciences and Technology of China (863 Program, 2013AA06A208), the Science and Technology Service Network Initiative of Chinese Academy of Sciences (STS, KFJ-EW-STS-091), and the National Science Foundation of China (41471404 and 51309214) were greatly acknowledged.

References

- Ahmad M, Lee SS, Oh SE, Mohan D, Moon DH, Lee YH, Ok YS (2013) Modeling adsorption kinetics of trichloroethylene onto biochars derived from soybean stover and peanut shell wastes. *Environ Sci Pollut Res* 20(12):8364–8373
- Ahmad M, Rajapaksha AU, Lim JE, Zhang M, Bolan N, Mohan D, Vithanage M, Lee SS, Ok YS (2014) Biochar as a sorbent for contaminant management in soil and water: a review. *Chemosphere* 99:19–33
- Baldock JA, Smernik RJ (2002) Chemical composition and bioavailability of thermally, altered *Pinus resinosa* (Red pine) wood. *Org Geochem* 33(9):1093–1109
- Beesley L, Moreno-Jimenez E, Gomez-Eyles JL (2010) Effects of biochar and greenwaste compost amendments on mobility, bioavailability and toxicity of inorganic and organic contaminants in a multi-element polluted soil. *Environ Pollut* 158(6):2282–2287
- Ben Yahia M, Knani S, Dhaou H, Hachicha MA, Jemni A, Ben Lamine A (2013) Modeling and interpretations by the statistical physics formalism of hydrogen adsorption isotherm on $\text{LaNi}_{4.75}\text{Fe}_{0.25}$. *Int J Hydrog Energy* 38:536–542
- Bopp C, Christl I, Schulin R, Evangelou MWH (2016) Biochar as possible long-term soil amendment for phytostabilisation of TCE-contaminated soils. *Environ Sci Pollut Res* 23(17):17449–17458
- Cabal B, Ania CO, Parra JB, Pis JJ (2009) Kinetics of naphthalene adsorption on an activated carbon: comparison between aqueous and organic media. *Chemosphere* 76:433–438
- Cao X, Ma L, Gao B, Harris W (2009) Dairy-manure derived biochar effectively sorbs lead and atrazine. *Environ Sci Technol* 43(9):3285–3291
- Cao XY, Pignatello JJ, Li Y, Latta C, Chappell MA, Chen N, Miller LF, Mao JD (2012) Characterization of wood chars produced at different temperatures using advanced solid-state C-13 NMR spectroscopic techniques. *Energy Fuel* 26(9):5983–5991
- Chefetz B (2003) Sorption of phenanthrene and atrazine by plant cuticular fractions. *Environ Toxicol Chem* 22:2492–2498
- Chefetz B, Xing B (2009) Relative role of aliphatic and aromatic moieties as sorption domains for organic compounds: a review. *Environ Sci Technol* 43(6):1680–1688
- Chefetz B, Deshmukh A, Hatcher PG, Guthrie EA (2000) Pyrene sorption by natural organic matter. *Environ Sci Technol* 34:2925–2930
- Chen BL, Xing BS (2005) Sorption and conformational characteristics of reconstituted plant cuticular waxes on montmorillonite. *Environ Sci Technol* 39(21):8315–8323
- Chen BL, Yuan MX (2011) Enhanced sorption of polycyclic aromatic hydrocarbons by soil amended with biochar. *J Soils Sed* 11(1):62–71
- Chen W, Duan L, Zhu D (2007) Adsorption of polar and nonpolar organic chemicals to carbon nanotubes. *Environ Sci Technol* 41(24):8295–8300
- Chen BL, Zhou D, Zhu L (2008) Transitional adsorption and partition of nonpolar and polar aromatic contaminants by biochars of pine needles with different pyrolytic temperatures. *Environ Sci Technol* 42(14):5137–5143
- Chen ZM, Chen BL, Chiou CT (2012) Fast and slow rates of naphthalene sorption to biochars produced at different temperatures. *Environ Sci Technol* 46(20):11104–11111
- Chen CP, Cheng CH, Huang YH, Chen CT, Lai CM, Menyailo OV, Fan LJ, Yang YW (2014) Converting leguminous green manure into biochar: changes in chemical composition and C and N mineralization. *Geoderma* 232:581–588
- Chio H, Al-Abed SR (2009) PCB congener sorption to carbonaceous sediment components: macroscopic comparison and characterization of sorption kinetics and mechanism. *J Hazard Mater* 165:860–866

- Chun Y, Sheng GY, Chiou CT, Xing BS (2004) Compositions and sorptive properties of crop residue-derived chars. *Environ Sci Technol* 38(17):4649–4655
- Cotoruelo LM, Marques MD, Rodriguez-Mirasol J, Rodriguez JJ, Cordero T (2009) Lignin-based activated carbons for adsorption of sodium dodecylbenzene sulfonate: equilibrium and kinetic studies. *J Colloid Interface Sci* 332(1):39–45
- Fagan SB, Souza AG, Lima JOG, Mendes J, Ferreira OP, Mazali IO, Alves OL, Dresselhaus MS (2004) 1,2-dichlorobenzene interacting with carbon nanotubes. *Nano Lett* 4(7):1285–1288
- Fu P, Hu S, Sun LS, Xiang J, Yang T, Zhang AC, Zhang JY (2009) Structural evolution of maize stalk/char particles during pyrolysis. *Bioresour Technol* 100(20):4877–4883
- Hale SE, Hanley K, Lehmann J, Zimmerman AR, Cornelissen G (2011) Effects of chemical, biological, and physical aging as well as soil addition on the sorption of pyrene to activated carbon and biochar. *Environ Sci Technol* 45(24):10445–10453
- Han L, Qian LB, Yan JC, Chen MF (2016) Contributions of different biomass components to the sorption of 1,2,4-trichlorobenzene under a series of pyrolytic temperatures. *Chemosphere* 156:262–271
- Kang S, Xing BS (2005) Phenanthrene sorption to sequentially extracted soil humic acids and humins. *Environ Sci Technol* 39:134–140
- Keiluweit M, Nico PS, Johnson MG, Kleber M (2010) Dynamic molecular structure of plant biomass-derived black carbon (biochar). *Environ Sci Technol* 44(4):1247–1253
- Khalfouli M, Knani S, Hachicha MA, Ben Lamine A (2003) New theoretical expressions for the five adsorption type isotherms classified by BET based on statistical physics treatment. *J Colloid Interface Sci* 263:350–356
- Khalfouli M, Baouab MHV, Gauthier R, Ben Lamine A (2006) Acid dye adsorption onto cationized polyamide fibres. Modeling and consequent interpretations of model parameter behaviours. *J Colloid Interface Sci* 296(2): 419–427
- Knani S, Mathlouthi M, Ben Lamine A (2007) Modeling of the psychophysical response curves using the grand canonical ensemble in statistical physics. *Food Biophys* 2:183–192
- Koltowski M, Hilber I, Bucheli TD, Oleszczuk P (2016) Effect of activated carbon and biochars on the bioavailability of polycyclic aromatic hydrocarbons in different industrially contaminated soils. *Environ Sci Pollut Res* 23(11):11058–11068
- Lattao C, Cao X, Mao J, Schmidt-Rohr K, Pignatello JJ (2014) Influence of molecular structure and adsorbent properties on sorption of organic compounds to a temperature series of wood chars. *Environ Sci Technol* 48(9):4790–4798
- Lee JW, Kidder M, Evans BR, Paik S, Buchanan AC III, Garten CT, Brown RC (2010) Characterization of biochars produced from cornstovers for soil amendment. *Environ Sci Technol* 44(20): 7970–7974
- Lehmann J (2007) A handful of carbon. *Nature* 447(7141):143–144
- Li L, Quinlivan PA, Knappe DRU (2002) Effects of activated carbon surface chemistry and pore structure on the adsorption of organic contaminants from aqueous solution. *Carbon* 40:2085–2100
- Li JF, Li YM, Wu YL, Zheng MY (2014) A comparison of biochars from lignin, cellulose and wood as the sorbent to an aromatic pollutant. *J Hazard Mater* 280:450–457
- Liao Y, Ma T, Cui Y, Qi Z (2014) Spatial distribution characteristics of volatile halogenated hydrocarbons in unsaturated zone of Xiaodian sewage irrigation area, Taiyuan, China. *Ecotoxicology* 23(10): 1951–1957
- Liu Z, Zhang FS, Wu J (2010) Characterization and application of chars produced from pinewood pyrolysis and hydrothermal treatment. *Fuel* 89(2):510–514
- Liu WJ, Jiang H, Yu HQ (2015) Development of biochar-based functional materials: toward a sustainable platform carbon material. *Chem Rev* 115(22):12251–12285
- Luo F, Song J, Xia WX, Dong MG, Chen MF, Soudek P (2014) Characterization of contaminants and evaluation of the suitability for land application of maize and sludge biochars. *Environ Sci Pollut Res* 21(14):8707–8717
- Ma XM, Anand D, Zhang XF, Talapatra S (2011) Adsorption and desorption of chlorinated compounds from pristine and thermally treated multiwalled carbon nanotubes. *J Phys Chem C* 115(11):4552–4557
- Nguyen TH, Cho HH, Poster DL, Ball WP (2007) Evidence for a pore-filling mechanism in the adsorption of aromatic hydrocarbons to a natural wood char. *Environ Sci Technol* 41(4):1212–1217
- Pastor-Villegas J, Rodriguez JMM, Pastor-Valle JF, Garcia MG (2007) Changes in commercial wood charcoals by thermal treatments. *J Anal Appl Pyrolysis* 80(2):507–514
- Pelekani C, Snoeyink VL (2000) Competitive adsorption between atrazine and methylene blue on activated carbon: the importance of pore size distribution. *Carbon* 38(10):1423–1436
- Qian LB, Chen BL (2013) Dual role of biochars as adsorbents for aluminum: the effects of oxygen-containing organic components and the scattering of silicate particles. *Environ Sci Technol* 47(15):8759–8768
- Qian LB, Zhang W, Yan J, Han L, Gao W, Liu R, Chen M (2016) Effective removal of heavy metal by biochar colloids under different pyrolysis temperatures. *Bioresour Technol* 206:217–224
- Ran Y, Yang Y, Xing B, Pignatello JJ, Kwon S, Su W, Zhou L (2013) Evidence of micropore filling for sorption of nonpolar organic contaminants by condensed organic matter. *J Environ Qual* 42(3):806–814
- Roberts KG, Gloy BA, Joseph S, Scott NR, Lehmann J (2010) Life cycle assessment of biochar systems: estimating the energetic, economic, and climate change potential. *Environ Sci Technol* 44(2):827–833
- Schmidt MWI, Noack AG (2000) Black carbon in soils and sediments: analysis, distribution, implications, and current challenges. *Glob Biogeochem Cycles* 14(3):777–793
- Sellaoui L, Guedidi H, Knani S, Reinert L, Duclaux L, Ben Lamine A (2015) Application of statistical physics formalism to the modeling of adsorption isotherms of ibuprofen on activated carbon. *Fluid Phase Equilib* 387:103–110
- Sellaoui L, Knani S, Erto A, Hachicha MA, Ben Lamine A (2016) Equilibrium isotherm simulation of tetrachlorethylene on activated carbon using the double layer model with two energies: steric and energetic interpretations. *Fluid Phase Equilib* 387:259–264
- Sharma RK, Wooten JB, Baliga VL, Martoglio-Smith PA, Hajaligol MR (2002) Characterization of char from the pyrolysis of tobacco. *J Agric Food Chem* 50(4):771–783
- Song Y, Wang F, Bian YR, Zhang YP, Jiang X (2012) Chlorobenzenes and organochlorinated pesticides in vegetable soils from an industrial site, China. *J Environ Sci (China)* 24(3):362–368
- Song Y, Wang F, Kengara FO, Yang X, Gu C, Jiang X (2013) Immobilization of chlorobenzenes in soil using wheat straw biochar. *J Agric Food Chem* 61(18):4210–4217
- Sun K, Jin J, Keiluweit M, Kleber M, Wang Z, Pan Z, Xing B (2012) Polar and aliphatic domains regulate sorption of phthalic acid esters (PAEs) to biochars. *Bioresour Technol* 118:120–127
- Tan X, Liu Y, Zeng G, Wang X, Hu X, Gu Y, Yang Z (2015) Application of biochar for the removal of pollutants from aqueous solutions. *Chemosphere* 125:70–85
- Wang XL, Xing BS (2007a) Importance of structural makeup of biopolymers for organic contaminant sorption. *Environ Sci Technol* 41(10): 3559–3565
- Wang XL, Xing BS (2007b) Sorption of organic contaminants by biopolymer-derived chars. *Environ Sci Technol* 41(24):8342–8348
- Wang XL, Cook R, Tao S, Xing BS (2007) Sorption of organic contaminants by biopolymers: role of polarity, structure and domain spatial arrangement. *Chemosphere* 66(8):1476–1484
- Wang Y, Hu YT, Zhao X, Wang SQ, Xing GX (2013) Comparisons of biochar properties from wood material and crop residues at different temperatures and residence times. *Energy Fuel* 27(10):5890–5899

- Wang B, Chen W, Fu H, Qu X, Zheng S, Xu Z, Zhu D (2014) Comparison of adsorption isotherms of single-ringed compounds between carbon nanomaterials and porous carbonaceous materials over six-order-of-magnitude concentration range. *Carbon* 79:203–212
- Xiao F, Pignatello JJ (2015) $\pi(+)$ - π interactions between (hetero) aromatic amine cations and the graphitic surfaces of pyrogenic carbonaceous materials. *Environ Sci Technol* 49(2):906–914
- Xiao L, Bi E, Du B, Zhao X, Xing C (2013) Surface characterization of maize-straw-derived biochars and their sorption performance for MTBE and benzene. *Environ Earth Sci* 71(12):5195–5205
- Xing BS (2001) Sorption of naphthalene and phenanthrene by soil humic acids. *Environ Pollut* 111:303–309
- Yang GP, Yang B, Lu XL, Ding HB, He Z (2014) Spatio-temporal variations of sea surface halocarbon concentrations and fluxes from southern Yellow Sea. *Biogeochemistry* 121(2):369–388
- Zhang GX, Zhang Q, Sun K, Liu XT, Zheng WJ, Zhao Y (2011) Sorption of simazine to corn straw biochars prepared at different pyrolytic temperatures. *Environ Pollut* 159(10):2594–2601
- Zhu DQ, Pignatello JJ (2005) Characterization of aromatic compound sorptive interactions with black carbon (charcoal) assisted by graphite as a model. *Environ Sci Technol* 39(7):2033–2041
- Zhu DQ, Hyun SH, Pignatello JJ, Lee LS (2004) Evidence for π - π electron donor-acceptor interactions between π -donor aromatic compounds and π -acceptor sites in soil organic matter through pH effects on sorption. *Environ Sci Technol* 38(16):4361–4368
- Zhu DQ, Kwon S, Pignatello JJ (2005) Adsorption of single-ring organic compounds to wood charcoals prepared under different thermochemical conditions. *Environ Sci Technol* 39(11):3990–3998